Journal of the Atmospheric Sciences

A Study of the Impacts of Vertical Diffusion on the Structure and Intensity of the Tropical Cyclones Using the High Resolution HWRF system

--Manuscript Draft--

Manuscript Number:	
Full Title:	A Study of the Impacts of Vertical Diffusion on the Structure and Intensity of the Tropical Cyclones Using the High Resolution HWRF system
Article Type:	Article
Corresponding Author:	Sundararaman Gopalakrishnan, Ph.D NOAA/ Atlantic Oceanographic and Meteorological Laboratory Miami, Florida UNITED STATES
Corresponding Author's Institution:	NOAA/ Atlantic Oceanographic and Meteorological Laboratory
First Author:	Sundararaman Gopalakrishnan, Ph.D
All Authors:	Sundararaman Gopalakrishnan, Ph.D
	Frank Marks, Ph.D
	Jun Zhang, Ph.D
	Xuejin Zhang, Ph.D
	Jian-Wen Bao, Ph.D
	Vijay Tallapragada, Ph.D
Abstract:	The Hurricane Weather Research and Forecasting system (HWRF) was used in an idealized framework to gain a fundamental understanding of the influence of vertical diffusion on the dynamics of tropical cyclone (TC) vortex intensification in three dimensions. The modeling system uses a simple scheme where the eddy diffusivity for momentum, heat and moisture are parameterized in terms of a closure that is dependent on the surface layer information and a profile depicting mixing above the layer. Flight-level data collected by a NOAA-P3 research aircraft during the eyewall penetration of category 5 Hurricane Hugo (1989) at an altitude of about 450-500 m and Hurricane Allen (1980) were used as the basis to best match the modeled eddy diffusivities with wind speed. While reduction of the eddy diffusivity to a quarter of its original value produced the best match with the observations, such a reduction revealed a significant decrease in the height of the inflow layer as well which, in turn, drastically impacted the size and intensity changes in the modeled TC. The cross-isobaric flow (inflow) was observed to be stronger with the decrease in the inflow depth. Stronger inflow not only increased the spin of the storm, enhancing the generalized Coriolis term in the equations of motion for tangential velocity, but also resulted in enhanced thetae in the boundary layer, a stronger and warmer core and, subsequently, a stronger storm. More importantly, rapid acceleration of the inflow not only produced a stronger outflow at the top of the inflow layer, more consistent with observations, but also a smaller inner core.
Suggested Reviewers:	Michel montgomery, Ph.D Professor, Naval Postgraduate School mtmontgo@nps.edu Expertise in the area of work
	Scott Braun, Ph.D Research Meteorologist, NASA Goddard scott.a.braun@nasa.gov Expertise in this area of work
	Hugh Willoughby, Ph.D Distinguished Research Professor, Florida International University hugh.willoughby@fiu.edu Expertise in the field
	Robert Tuleya, Ph.D

	Robert Tuleya, Ph.D Senior Scientist/NOAA/GFDL &tResearch Professor, Old Dominion University Robert.Tuleya@noaa.gov Expertise in the field
	Roger Smith, Ph.D Professor, University of Munich, Germany roger.smith@lmu.de Expertise in the area of work
	Morris Bender Senior Scientist, GFDL/NOAA morris.bender@noaa.gov Expertise in this field
	Yi Jin, Ph.D Scientist, Naval Research Labratory, Monterey,CA yi.jin@nrlmry.navy.mil Expertise in the area of work
	David Nolan Professor, University of Miami dnolan@rsmas.miami.edu Expertise in the field
	Michel Bell, Ph.D Naval Postgraduate School mmbell@nps.edu Expertise in the area
	Da-Lin Zhang, Ph.D Professor, University of Maryland dalin@atmos.umd.edu Expertise in the area
	Yuqing WANG Professor, University of Hawaii yuqing@hawaii.edu Expertise in the area of work

The Editor Date: Dec 18, 2011

Journal Of the Atmospheric Sciences

Dear Editor,

Please find enclosed our manuscript entitled “A Study of the Impacts of Vertical Diffusion on the Structure and Intensity of the Tropical Cyclones Using the High Resolution HWRF system by Gopalakrishnan et al.”. We wish to submit the above manuscript for a review. Please do not hesitate to contact me if there is an issue with the follow up process.

Regards

gopal
Sundarar Gopalakrishnan, Ph.D
Meteorologist/Hurricane Modeling Team Leader
Hurricane Research Division/AOML/NOAA
gopal@noaa.gov

Page and Color Charge Estimate Form

Click here to download Page and Color Charge Estimate Form: Page_Charge_Estimation_Form.pdf

A Study of the Impacts of Vertical Diffusion on the Structure and Intensity of the Tropical Cyclones Using the High Resolution HWRF system

Sundararaman G. Gopalakrishnan[1], Frank Marks, Jr[1], Jun A. Zhang[2], Xuejin Zhang[2], Jian-Wen Bao[3] and Vijay Tallapragada[4]

[1] NOAA/ Atlantic Oceanographic and Meteorological Laboratory/ Hurricane Research Division, Miami, FL, USA;

[2] University of Miami, Cooperative Institute for Marine and Atmospheric Studies, Miami, FL, USA;

[3] NOAA/Earth System Research Laboratory
Boulder, CO, USA;

[4] NOAA/Environmental Modeling Center, National Centers for Environmental Predictions, Washington, DC, USA

(Submitted to the Journal of the Atmospheric Sciences: December 19, 2011)

Corresponding author address: S.G. Gopalakrishnan, AOML/HRD, 4301 Rickenbacker Causeway, Miami, Florida 33149 <E-mail: gopal@noaa.gov>

Abstract

The Hurricane Weather Research and Forecasting (HWRF) system was used in an idealized framework to gain a fundamental understanding of the influence of vertical diffusion on the dynamics of tropical cyclone (TC) vortex intensification in three dimensions. The modeling system uses the so-called Medium-Range Forecast (MRF) parameterization scheme where the eddy diffusivity for momentum is parameterized as $Km = k\,(U_*/\Phi_m)\,Z\,(1 - Z/h)^2$ in which k is the von Karman constant, U_* is the surface frictional velocity scale, Φ_m is the wind profile function evaluated at the top of the surface layer, Z is the height above the surface, and h is the boundary layer height. The eddy diffusivity of heat and moisture, Kh, was computed from Km using the relationship of the Prandtl number. Flight-level data collected by a NOAA WP-3D research aircraft during the eyewall penetration of category 5 Hurricane Hugo (1989) at an altitude of about 450-500 m (Marks et al. 2008) and Hurricane Allen (1980) (Marks 1985) were used as the basis to best match the modeled eddy diffusivities with wind speed. While reduction of the eddy diffusivity to a quarter of its original value produced the best match with the observations, such a reduction revealed a significant decrease in the height of the inflow layer as well which, in turn, drastically impacted the size and intensity changes in the modeled TC. The cross-isobaric flow (inflow) was observed to be stronger with the decrease in the inflow depth. Stronger inflow not only increased the spin of the storm, enhancing the generalized Coriolis term in the equations of motion for tangential velocity, but also resulted in enhanced θe in the boundary layer, a stronger and warmer core and, subsequently, a stronger storm. More importantly, rapid acceleration of the inflow not only produced a stronger outflow at the top of the inflow layer, more

consistent with observations, but also a smaller inner core. For instance, while the radius of maximum wind speed at the first model level was 42 km in the simulation using the original MRF scheme, it decreased to about 31 km when the value of eddy diffusivity was decreased to a quarter of the original value.

1. Introduction

The upward transfer of moisture and heat from the ocean surface to the atmosphere and the downward transfer of momentum from the atmosphere to the ocean surface by turbulence mixing processes within the hurricane boundary layer[1] have long been known to play an important role in regulating the radial and vertical distribution of enthalpy and momentum and, consequently, intensity changes in tropical cyclones (e.g., Malkus and Riehl 1960; Rosenthal 1962; Smith 1968; Ooyama 1969; Kurihara and Tuleya 1974; Anthes and Chang 1978; Tuleya and Kurihara 1978; Emanuel 1986, 1995). In fact, as early as in the 1960s, Smith (1968) used a simple analytical model to examine some of the features of the hurricane boundary layer by varying the eddy diffusivities. He concluded, however, that inadequate knowledge of the turbulence structure at that time prevented a more realistic understanding of the layer. To date, even with the best forecast models for tropical cyclone (TC) prediction operating at the highest resolution it is still not possible to resolve these transport and diffusive processes in the lower atmosphere. Hence, subgrid scale parameterization schemes are required. These parameterization schemes are usually dependent on four key parameters, namely, surface exchange coefficients for momentum (Cd), moisture and heat (Ck), eddy diffusivity for momentum (Km), and moisture and heat (Kh). These parameters determine the transfer

[1] In the context of this text the Ekman layer or the inflow layer is taken to be the height of the hurricane boundary layer.

and diffusion of fluxes from the atmosphere to the underlying ocean surface and vice-versa. However, there is a large degree of uncertainty in the estimates of these parameters. Consequently, the structure and intensification of TCs as simulated by high-resolution mesoscale models are sensitive to the surface and planetary boundary layer (PBL) parameterizations used in these models (e.g., Braun and Tao 2000; Nolan et al. 2009a,b; Montgomery et al. 2010; Smith and Thomsen 2010).

Until recently, direct measurements of surface fluxes for computation of Cd and Ck in the inner-core region of intense hurricanes were nonexistent, and it is no surprise that, even for the same storm, different surface layer parameterization schemes yield a diverse range of structure and intensity predictions (see, for example, Figs. 9 and 16 in Braun and Tao 2000). In 2003, Powell et al. reported an important observational finding for the high wind regime. Their work suggested that Cd decreases at wind speeds above 40 m s^{-1} rather than increasing as parameterized in numerical models at that time. Donelan et al. (2004) presented strong evidence to confirm that at high wind speeds Cd ceases to increase with wind speed. At the same time, based on wind stress data obtained from the National Oceanic and Atmospheric Administration (NOAA)/National Centers for Environmental Prediction (NCEP) surface wave model WAVEWATCH-III, Moon et al. (2004a,b) reported similar findings that established the Cd behavior in hurricanes. Presently, however, the high wind speed behavior of Ck is still lacking strong observational support. Nevertheless, a synthesis of observations from the Coupled Boundary Layer Air-Sea Transfer Experiment (CBLAST) (Black et al. 2007; Zhang 2007; Zhang et al. 2008) provides evidence on the observed behavior of Ck in moderate wind regions, especially between 15-30 m s^{-1}. Recent laboratory experiments (Haus et al.

2010) and the theoretical study of Montgomery et al. (2010) also present additional evidence to confirm a constant behavior of Ck above wind speeds of about 30 m s^{-1}. A value of about 1.2-1.3 x 10^{-3} for Ck appears to be a reasonable estimate.

Flight-level data collected by a NOAA WP-3D research aircraft during the eyewall penetration of category 5 Hurricane Hugo (1989) at an altitude of about 450-500 m (Marks et al. 2008) and Hurricane Allen (1980) (Marks 1985) provide a unique opportunity for estimating eddy diffusivities. These estimates are important for evaluating numerical models. Based on an analysis of the flight-level data for these two intense storms, Zhang et al. (2011a) provided estimates of the eddy diffusivity coefficient in the hurricane boundary layer with the maximum Km (and Kh) values varying between 38-101 m^2 s^{-1}. These estimates are consistent with estimates from the theoretical and numerical studies of Kepert (2001) and Smith (2003). More recently, Zhang et al. (2011b) used data from 794 GPS dropsondes deployed by NOAA research aircraft in 13 hurricanes to study the characteristic height scale of the hurricane PBL. A composite analysis from their study demonstrates that the height of the inflow layer increases with increasing radius from the center of strong storms (categories 4-5 on the Saffir-Simpson scale, with a minimum inflow layer depth of about 900 m near the eye to about 1200 m at a distance of about five times the radius of the maximum wind. These data sets are used to evaluate the surface and PBL parameterizations in the Hurricane Weather Research and Forecast (HWRF) system described here.

A simple first-order vertical diffusion parameterization scheme based on the local Richardson number for determining Km and Kh has been in use in NCEP's Medium-Range Forecast (MRF) model since the 1980s, and an upgraded version based on the

non-local K approach valid within the well-mixed boundary layer (Hong and Pan 1996) has been used in the Global Forecasting System (GFS) since the 1990s. The MRF scheme is also used in a suite of operational models such as the Geophysical Fluid Dynamics Laboratory's (GFDL) hurricane model and the HWRF system, among others. The MRF scheme has also been a popular option in research models such as the fifth-generation NCAR/Pennsylvania State University mesoscale model (MM5). Braun and Tao (2000) studied the sensitivity of high-resolution simulations of Hurricane Bob (1991) to PBL parameterizations. This study used four PBL parameterization schemes (namely, a simple bulk aerodynamic scheme, a local Richardson number and mixing length based Blackadar scheme, the MRF, and a high-order, Turbulence Kinetic Energy based Burk–Thompson boundary layer scheme) and compared their eyewall structure, storm intensity, and boundary layers, illustrating the sensitivity of surface exchange and subsequent vertical mixing processes on TC structure and intensity predictions. The study also found that the MRF scheme in MM5 produced weaker and deeper inflow and that the strong outflow at the top of the PBL was absent when compared to the other schemes. Additionally, the MRF scheme produced the weakest storm.

Recently, several studies (e.g., Nolan et al. 2009a,b; Smith and Thomsen, 2010 and Bao et al. 2011) have illustrated the sensitivity of modeled surface and PBL schemes to hurricane structure and intensity predictions. For instance, Nolan et al. (2009a,b) provided an extensive evaluation of PBL parameterizations in TCs by comparing in situ observations to high-resolution simulations of Hurricane Isabel (2003). In particular, the authors used the Yonsei University (YSU) parameterization and the Mellor–Yamada–Janjic (MYJ) parameterization available within the Weather Research and Forecasting

(WRF) modeling framework. They found that by modifying the original YSU and MYJ schemes to ocean roughness lengths more in agreement with previous observations (Donelan et al. 2004), improved predictions were possible for the simulation of Hurricane Isabel, as measured by standard metrics of track and 10-m winds. When compared with CBLAST observations obtained during Hurricane Isabel, both schemes reproduced the structure remarkably well. Nevertheless, the authors did notice differences in the structure modeled by the two schemes. Smith and Thomsen (2010) demonstrated a dependence of tropical cyclone intensification on the boundary-layer representation in MM5. Predictions using one of five available schemes were compared, not only amongst themselves but, where possible, with recent observational analyses of the boundary-layer structure. Although the study identified shortcomings of the individual schemes (e.g., the MRF scheme), it fell short of advocating the use of a particular scheme. The authors concluded that the current inability to determine "the optimum scheme" had implications for the predictability of tropical cyclone intensification.

Although it is clear from the above discussions that modeled TC structure and intensity predictions are known to be sensitive to PBL parameterization schemes, it is unclear why a particular scheme behaves differently when compared to another or what might be a case independent, optimal choice for improving TC numerical forecasts. To address these issues, we focused our efforts on the fundamental source of variability in the structure and intensity prediction in high resolution numerical models, namely, vertical eddy diffusivity. Specifically, in this work we studied the impacts of modifying Km (and Kh), consistent with the observed flight-level data from mature storms, on the structure and intensification of an idealized vortex within the framework of the HWRF

system. We used the MRF scheme because of its simplicity to the TC forecasting problem and its use in NCEP operational models. To the best of our knowledge, this is the first time a synthesis of flight-level observations has been used as the basis to provide an improvement to the existing boundary layer parameterization scheme in a high resolution hurricane model. The study also provides a fundamental understanding on the size, structure, and subsequent intensification of modeled storms.

2. The HWRF Model, Configuration, and Physics

The HWRF system was developed at NOAA's National Weather Service (NWS)/NCEP to address the Nation's next generation hurricane forecast problems and became an operational track and intensity guidance tool in 2007. A version of this evolving system is available at the Development Testbed Center (DTC), National Center for Atmospheric Research (NCAR), in Boulder, Colorado, and the scientific documentation (Gopalakrishnan et al. 2010) is available at http://www.dtcenter.org/HurrWRF/users/docs/scientific_documents/__HWRF_final_2-2_cm.pdf. An experimental version of the HWRF system (dubbed as HWRFX) was specifically adopted and developed at the Hurricane Research Division (HRD) of the Atlantic Oceanographic and Meteorological Laboratory (AOML) to study the intensity change problem at cloud-resolving scales (about 1-3 km). This modeling system is supported by NOAA's Hurricane Forecast Improvement Project (HFIP) and complements the operational HWRF system. HWRFX can be run both in real (Zhang et al. 2011; Yeh et al. 2011; Pattanayak et al. 2011) and idealized frameworks (Gopalakrishnan et al. 2011a). Until recently, we developed and tested new techniques with HWRFX that evaluated their potential to improve hurricane forecasts before they became formally adopted for

use within HWRF. However, as the research and operational communities collaborated under the auspices of HFIP to improve tropical cyclone intensity forecasts, we realized the need to merge the two systems. The merger of the experimental and operational systems, HWRFV3.2, was used in the current study.

. In this work, we used the triply-nested version of the HWRFV3.2 system (X. Zhang, personal communication). The model is configured with a coarse mesh of 27 km horizontal grid spacing covering about 50 x 50 degrees and two, two-way telescopic moving nests at 9 km covering about 15 x 15 degrees and 3 km covering about 5 x 5 degrees, respectively. There are 42 hybrid levels with at least 10 levels below the 850-mb level. Recently, HWRFX was used in an idealized framework to gain a fundamental understanding of the influence of horizontal grid resolution on the dynamics of hurricane vortex intensification in three dimensions (Gopalakrishnan et al. 2011a). We used the same ideal initialization in this work. Described in brief, the non-linear balance equation in the pressure-based sigma coordinate system described in Wang (1995) was solved within the rotated latitude-longitude E-grid framework, where the mass field was obtained from the wind field. The calculations were performed on an f-plane centered at 15^0. The model was initialized with an axisymmetric cyclonic vortex of initial strength of 20 m s^{-1} with a radius of maximum wind of about 90 km, embedded in a uniform easterly flow of 4 m s^{-1}. The far field temperature and humidity were based on Jordan's Caribbean sounding (Gray et al. 1975). In all of the experiments, the sea surface temperature was set to 302 K, and no land was present anywhere in the domain.

The model physics options used in this study were configured as close as possible to the operational HWRF system. An extensive overview of the physics packages used in

the HWRF system is provided in Gopalakrishnan et al. (2010) and Yeh et al. (2011) and only briefly discussed here. The Ferrier scheme (Ferrier et al. 2002) was used to provide latent heating to resolve the grid scale microphysical processes in the atmosphere, and the Simplified Arakawa and Schubert scheme, also known as the SAS scheme (Pan and Wu 1995; Hong and Pan 1998), was used to parameterize subgrid cumulus-cloud activity. Cumulus parameterizations in combination with the Ferrier microphysical scheme have been found to have some value in the operational Non-Hydrostatic Mesoscale Model (NMM) for scales down to about 3-5 km (Gopalakrishnan et al. 2011a). In this study, we retained SAS convection in all three domains. The GFDL long wave radiation scheme that follows the simplified exchange method of Fels and Schwarzkopf (1975) and Schwarzkopf and Fels (1991) and the short-wave radiation of Lacis and Hansen (1974) were also used in the current study.

The HWRF system uses the GFDL surface layer parameterization scheme. Based on the Monin-Obukhov similarity theory, the parameterization scheme provides estimates[2] of the surface layer exchange coefficients, Cd and Ck, for further computation of the surface layer fluxes. Since the 2006 GFDL model upgrades, the Cd values computed in the scheme have provided estimates consistent with observations for both higher and lower wind speeds (Bender et al. 2007). However, largely due to uncertainties in the observations, Ck was left unchanged (Fig. 3 in Bender et al. 2007). Until the 2009 hurricane season, the HWRF system used the GFDL implementation of the surface layer scheme. However, based on more recent laboratory experiments (Haus et al. 2010) the upgraded operational HWRF system in 2010 used a constant value of 1.3×10^{-3} for Ck.

[2] *In advanced numerical models, the exchange coefficients are a function of stability and the roughness lengths for momentum, heat, and moisture.*

Figures 1a and 1b provide an estimate of Cd and Ck, respectively, obtained from one of the simulations reported here. The simulated values obtained from the 72nd hour of the forecast representing a mature storm were compared with currently available observations. With the 2010 surface layer upgrades, we believe the HWRF system provides a reasonable parameterized estimate of the surface layer exchange coefficients within the range of the observational uncertainties.

The GFS boundary layer formulation (Hong and Pan 1996), which is the main topic of discussion in this study, was used to parameterize the flux transport and subsequent mixing in the atmosphere. In this scheme, the momentum eddy diffusivity is

$$Km = k\,(U_*/\Phi_m)\,Z\,\{\alpha(1 - Z/h)^2\}, \qquad (1)$$

where k is the von Karman constant (=0.4), U_* is the surface frictional velocity scale, Φ_m is the wind profile function evaluated at the top of the surface layer, Z is the height above the surface, and h is the boundary layer height. In the original formulation, which may be valid over land, α=1.0. In this study, we used a synthesis of observations from Zhang et al. (2011a,b) and conducted several sensitivity experiments by varying the value of α. However, since the differences were systematic only simulations of significance are reported in Table 1. Further, we evaluated the value of α that best provides estimates of the observed diffusivities and then studied the impacts of these changes on the structure and intensity changes of the ideal vortex. As discussed in Hong and Pan (1996), the eddy diffusivity for heat (and moisture), Kh, was computed from Km using the relationship of the Prandtl number. Finally, the numerical diffusivity along the horizontal direction was held fixed to a small background value in all the experiments. The input parameter that controls the lateral diffusion in the HWRF system is known as COAC (Gopalakrishnan,

2011b), and this parameter was set to 0.7 in all domains. This is the smallest suggested value for the NMM dynamic core.

3. Results and Discussion

3.1 Methodology of Analysis of the Results

All simulations reported in Table 1 were run for 96 hours. Apart from the examination of the time traces for the minimum mean sea-level pressure, 10-m wind speeds in the inner core, and eddy diffusivities for momentum (Km) that were isolated from the raw hourly output on the native grid system of the inner nest at 3-km resolution, we further divided our investigation into two parts. These parts included (i) an axisymmetric analysis of the output from the 3 km inner nest following Gopalakrishnan et al. (2011a), where the influence of horizontal resolution and physics on the structure and intensity changes in TCs using a similar idealized framework were studied, and (ii) a simple examination of the basic gradient wind equations that involved an iterative solution of the coupled equations for the radial and tangential components of wind (Stull 2000).

As illustrated in Zhang et al. (2001) and Gopalakrishnan et al. (2011a), it is convenient to discuss the axisymmetric inner-core dynamics in cylindrical coordinates (r, λ, z), where r is the distance from the center of the vortex, λ is the azimuthal angle, and z is the vertical height. The hourly output on the native grid from the model was transformed to the cylindrical polar height coordinate system. Further, for the sake of analysis, we recast the horizontal equations of motion into tangential momentum, governing the primary circulation and radial components that govern the secondary circulation for the HWRF system. The governing equations are:

$$\frac{dv_\lambda}{dt} = -\frac{1}{\rho r}\frac{\partial p}{\partial \lambda} - \underbrace{\frac{u_r v_\lambda}{r} - fu_r}_{\text{Term A}} + D_{v\lambda} \qquad (2)$$

$$\frac{du_r}{dt} = -\underbrace{\frac{1}{\rho}\frac{\partial p}{\partial r} + \frac{v_\lambda v_\lambda}{r} + fv_\lambda}_{\text{Term B}} + D_{ur} \qquad (3)$$

$$\text{Where } \frac{d}{dt} = \frac{\partial}{\partial t} + u_r\frac{\partial}{\partial r} + \frac{v_\lambda}{r}\frac{\partial}{\partial \lambda} + w\frac{\partial}{\partial z} \qquad (4)$$

In equations 2, 3, and 4, u_r, v_λ, and w are, respectively, the radial, tangential, and vertical winds in the earth-relative transformed coordinate system, p is the pressure, and Dv_λ and Du_r are, respectively, the diffusion (frictional) terms in the tangential and radial directions. Equation 2 is related to the "spin up" of the vortex, and Term A is known as the generalized Coriolis term. Its significance to the "spin up" process is discussed later in the text. Equation 3 represents the net forcing related to the secondary circulation. In the absence of friction and the net forces that constitute balance, equation 3 reduces to the gradient wind relationship (Term B). Equations (2) and (3) can be solved iteratively to gain a basic understanding of the boundary layer gradient wind flows with a simple approximation for the diffusion terms, i.e., when parameterized as a function of drag and the depth of the inflow layer (e.g., Stull 2000; Smith and Vogl 2008).

3.2 Time Series of the Vortex Developments

Figure 2 provides a time history of the intensification of the inner nest at 3-km resolution for the control run (A100), α of 0.50 (A050), and α of 0.25 (A025),

respectively, while Table 2 provides a snapshot of the storm statistics sampled from the entire life history of the storm. After an initial period of gestation, a period of rapid intensification is observed starting at about 12 hours for all three simulations and continuing almost up to 36 hours (Fig. 2a). During this time, the mean sea level pressure is reduced to 955 hPa in A100, 950 hPa in A050, and 940 hPa in A025. The MSLP at the end of the simulations are, respectively, 939 hPa, 925 hPa, and 919 hPa (Table 2). In addition, although the initial size of the radius of maximum winds for the storm in all three cases was set to 90 km, it is reduced rapidly during the model integration, with A025 producing the smallest inner core in the three cases (Fig. 2b). The minimum radius of maximum winds during its lifecycle for A100 was 36 km, whereas it was 27 km in A025 (Table 2). Figures 2c,d,e provide Hovemoller diagrams of the axisymmetric mean winds at a height of 10 m for A100, A050, and A025. The maximum tangential wind at any location in the storm during its lifetime for A100 was 70 m s^{-1}, whereas it was about 79 m s^{-1} for A025 (Table 2). Clearly, A025 produces the strongest inner core, as well as the smallest inner core[3]. We further analyzed the intensification process in light of these results. Gopalakrishnan et al. (2011a) provided an overview of the rapid intensification phase. In this study, we focus on the impact of the PBL on the behavior of the mature storm.

3.3 Comparison of Eddy Diffusivities with Observations

Figure 3 depicts the modeled variation of Km with wind speed for the control run (A100), α of 0.50 (A050), and α of 0.25 (A025), respectively. Flight-level observations from hurricanes Hugo and Allen presented in Zhang et al. (2011a) were compared with the

[3] As measured by the radius of maximum wind at the first model level (about 30 m) in this study.

modeled outputs at nearly the same height. Clearly consistent with the initial findings of Braun and Tao (2000), the original MRF scheme (A100) overestimates the values of Km. Nevertheless, more reasonable modeled estimates are produced after decreasing the α parameter. We trailed a string of values for α as small as 0.10 (not reported). The estimates produced in the A025 simulation, where Km was reduced to a quarter of its original value, provided the closest match with the observations (Fig. 3c). Reduction of vertical diffusion in the A050 and A025 simulations had a significant influence on the structure of the PBL and subsequent TC intensification process and will be discussed in the following section.

3.4 Structure and Intensification Process

Figure 4 shows the tangentially-averaged, 6-hourly time averaged, radius-height cross section of the secondary circulation centered around the 93rd hour of the simulations and represents the mean structure of a mature storm for the control run (A100), α of 0.50 (A050), and α of 0.25 (A025), respectively. As indicated by the vectors and contours in Fig. 4a, the circulation in the A100 simulation is characterized by a deep layer of radial inflow almost more than a couple of kilometers deep[4] in the lower troposphere and a layer of intense outflow characterizing the upper-level divergence at about 14 km height (not shown for the sake of clarity). The rising branch of the secondary circulation, depicted by green contours and located in the eyewall region, slopes radially outward. A *very weak* outflow is observed above the shallow inflow layer due to the return flow. The model is able to reproduce the same features as reported in Gopalakrishnan et al. (2011a). However, a comparison with the available observational data from Zhang et al. (2011b) indicates that the simulated inflow layer depth is at least twice the thickness of that observed.

[4] *The depth of the inflow in this study was taken to be the height where the radial wind velocity is reduced to about 3 ms^{-1}. Significant inflow above the boundary layer is not uncommon (e.g., Willoughby 1979).*

Nevertheless, more reasonable modeled estimates are produced after decreasing the α parameter. A comparison between A100 with A050 and A025 (Figs. 4a,b,c) indicates a systematic reduction of the inflow depth with a decrease in Km (and Kh) and an increase in the strength of the radial winds. The inflow layer in A100 is about 2.5 km, while it is about 1.5 km in A050 and reduces to the observed value of about 1 km in A025. As the depth of the inflow layer decreases, the strength of the inflow increases. While the maximum radial wind in A100 is about 15 m s^{-1}, it is about 21 m s^{-1} in A050 and about 27 m s^{-1} in A025. The radius of the maximum winds also shrink in size. While the radius at the first model level is 42 km in A100, it is 37 km in A050 and further reduces to 31 km in A025.

As mentioned in section 3.1, to further understand the influence of the inflow depth on the surface wind, a "toy model" was developed based on a simple balance/imbalance of forces along the horizontal direction in the PBL. Such a balance/imbalance of forces leads to the boundary-layer gradient (BLG) wind equations. The BLG wind equations, which are a coupled system (equations 2 and 3) with a simple approximation to the frictional term, were solved using an iterative procedure provided in Stull (2000). In this procedure, given the initial gradient wind in balance above the boundary layer, the bulk drag (Cd) within the boundary layer, and the inflow layer depth, the tangential wind adjusts to a new state due to the changing balance between the pressure gradient, and Coriolis, centrifugal, and turbulent drag forces within the boundary layer. In the process, a radial inflow is created even in this "toy model." Stull (2000) provides an example (chapter 9, pages 192-194) that we extended using inputs consistent with our work here to provide insights for this study. The gradient wind above the boundary layer was set to 50 m s^{-1} to represent a mature storm (as in Fig. 4), the Coriolis parameter was set to 0. 00015 s^{-1}, the radius of curvature was set to 1000 km to

describe the entire circulation, and Cd was set to 0.002 ($\pm$ 0.001). Although such simplified examples may not reproduce the structure and intensification processes discussed in this work, we found the example to be useful for explaining some of the observed sensitivities in our results from A100, A050, and A025 (Fig. 4). For instance, Fig. 5 provides the variation of the radial and tangential wind speeds with the depth of the inflow layer for three Cd values (with a mean of 0.002 from Fig. 1a). Clearly, with a decrease in the inflow layer depth, the strength of the tangential wind decreases but, more importantly, the radial inflow becomes stronger. While the speed of the radial velocity was as low as 5 m s^{-1} for an inflow depth of 4000 m and a Cd of 0.002, it increased threefold to 15 m s^{-1} when the depth was 1000 m. Changes in drag also had a noticeable effect on the radial inflow.

A reduction in vertical eddy diffusivity (Km and Kh) and the subsequent increase in the strength of the radial inflow have a significant influence on the structure and intensity of the TC. Figure 6 provides a Hovemoller diagram of the tangentially-averaged, 6-hourly time averaged radial component of velocity (in m s^{-1}). Superposed on the contour lines is the generalized Coriolis term (i.e., Term A in equation 2) *with the addition of a frictional effect* from equation 2 for the HWRF runs with (i) α=1 (A100), (ii) α=0.5 (A050), and (iii) α=0.25 (A025) runs at the 30-m level. The blue end of the spectrum represents tangential acceleration ("spin up"), and the red end of the spectrum represents deceleration. A comparison between Figs. 6a,b,c clearly indicates that the increase in inflow speed is coupled with the increase in generalized Coriolis and subsequent increase in tangential acceleration *despite friction* (equation 2). Montgomery and Smith and their colleagues used MM5 at a resolution of about 1.67 km to examine the basic process of intensification in an idealized vortex (see Montgomery and Smith 2011 for a summary).

These studies showed that the axisymmetric aspects of intensification involve not only the convergence of absolute angular momentum above the boundary layer but also the convergence of absolute angular momentum within the boundary layer. There is no significant difference between the inflow above the PBL for A100, A050, and A025 (Fig. 4). However, it is the systematic increases to the strength of the inflow within the PBL that results in noticeable differences in the "spin up" processes.

Figure 7 provides the Hovemoller diagram of the tangentially-averaged, 6-hourly time averaged radial θ_e at the 30-m level for the HWRF runs with (i) α=1 (A100), (ii) α=0.5 (A050), and (iii) α=0.25 (A025). The region of vertical motion exceeding the 0.2 m s^{-1} contour line at the top of the boundary layer is shown to indicate the approximate region of eyewall convection. Cram et al. (2007) studied the transport and mixing characteristics of a large sample of air parcels from Hurricane Bonnie (1998). He found that a portion of the low-level inflow from the hurricane bypassed the eyewall to enter the eye, and this air both replaced the mass of the low-level eye and lingered for a sufficient time (order 1 h) to acquire enhanced entropy characteristics through its interaction with the ocean beneath the eye, which enhanced the efficiency of the hurricane heat engine (Emanuel 1986). A comparison between Figs. 7a,b,c illustrates that in addition to the "spin up" of the primary circulation (Fig. 6), the enhanced strength of the cross-isobaric flow (Fig. 4) provides a mechanism for increased entropy within the boundary layer. Although the surface latent heat fluxes (and enthalpy) were reduced in A025 (not shown), the enhanced enthalpy caused by advection of moisture and heat above the surface layer was sufficient to produce a stronger hurricane.

Figure 8 provides a Hovemoller diagram of the tangentially averaged, 6-hourly time averaged radial component of velocity (in m s^{-1}). Superposed on the contour lines in colored shading is the net radial forcing term *including radial friction* from the governing equation for the secondary circulation (equation 3) of the HWRF runs with (i) α=1, (ii) α=0.5, and (iii) α=0.25 runs at the 30-m level. The blue end of the spectrum represents radial acceleration (convergence), and the red end of the spectrum represents deceleration within the inner eyewall region. Units of the net radial forcing term are in m s^{-1} h^{-1}. As indicated in Fig. 8a, the PBL and eyewall regions are characterized by imbalances in the gradient wind. These results are comparable with those of Gopalakrishnan et al. (2011a). However, it should be noted that the strength of the agradient forcing used in that study had to be rescaled for the current study because of the significant increase in the strength of the inflow, as well as the agradient forcing terms for the other runs in Table 1. The following points are worth noting:

- The evolution of a mature TC occurs through cooperative interaction between the primary and secondary circulations (Ooyama, 1969, 1982). The larger the departure from the gradient wind either by "spin up" of the primary circulation discussed in the above section or due to reduced radial frictional forces or both (refer to equation 3), the larger the acceleration in the eyewall and deceleration within the eye (equation 3). In an experiment with reduced drag, Montgomery et al. (2010) demonstrated that rapid acceleration of the inflowing air causes a greater agradient force and, hence, is converged farther inward before rising out of the boundary layer and ascending into the eyewall updraft. While decreased drag caused convergence farther inward in their study (see Fig. 2,

Montgomery et al. 2010), the strength of the inflow and the subsequent "spin up" *within the boundary layer* led to the imbalance and subsequent acceleration (and radial convergence) in the current study. Clearly for A025, the radial acceleration within the boundary layer was so strong (Fig. 8c) that a radial jet of 3 m s^{-1} was produced at about 1-1.5 km above the surface (Fig. 4c), consistent with the studies of Smith and Montgomery and coworkers (e.g., Smith et al. 2009; Montgomery et al. 2010), as well as other recent findings (Bell and Montgomery 2008).

- It is important to note that as the air is converged farther inward towards the eye in A100, A050, and A025 (Fig. 8), the size of the inner core, as defined here by the radius of maximum wind, decreases. For instance, while the radius of the maximum wind for a mature storm is about 41 km for A100 (Fig. 4a), it is reduced to about 37 km in A050 (A050) and to about 31 km in A025 (Fig. 4c).

4. Sensitivity Experiments

A good review of the external factors that may control the size of the storm, both in terms of the inner core and spiral rainbands and the diabatic heating outside the eyewall region, is provided in Xu and Wang (2010). From this study, it appears that the initial size of the storm, as well as the environmental relative humidity, may have some sensitivity on the inner core in the context of the results discussed above. Table 1 provides an overview of these sensitivity experiments (number 4 to 12).

Figure 9 depicts the Hovemoller diagram of the axisymmetric mean wind at 10 m (in color). Superposed are the contours of tangentially averaged, 6-hourly time averaged radial components of velocity (in m s^{-1}) at the 30-m level (i.e., first model level) for the HWRF runs with an initial radius of maximum wind set to 120 km (top row) and 60 km (middle row) and for (i) α=1 (B100 and S100), (ii) α=0.5 (B050 and S050), and (iii) α=0.25 (B025 and S025) runs (Table 1). The bottom row illustrates the importance of the environmental relative humidity for the three α values (RHA100, RHA050, and RHA025 in Table 1). Several features are worth noting:

- A comparison between B100, B050, and B025, or S100, S050, and S025, indicates that the tropical cyclone inner core size is critically dependent on the initial vortex size. A larger initial storm evolves to become a larger storm, and an initially smaller storm evolves to become even smaller. While the maximum radius of maximum wind was on the order of 70 km at 96 hours in B100 (Fig. 9a), the minimum size was as small as 13 km around 24 hours in S025 (Fig. 9f and Table 2).
- Xu and Wang (2010) found that strong outer winds in a storm with a larger initial size led to large entropy fluxes and to a large radial extent outside the eyewall, favoring the development of active spiral rainbands and, subsequently, larger (area wise) radial inflow and accelerating tangential winds outside the eyewall. These factors also led to an outward expansion of the tangential wind fields. On the contrary, based on the same argument, an initially small vortex remained weak and small in this study. The results in Fig. 9 are consistent with those from Xu and Wang (2010).

- More importantly, within the context of the current study, a comparison between B100, B050, and B025 (Figs. 9a,b,c) indicates that the eddy diffusivity has a significant influence on this class of big storms. There is a systematic increase in the strength of the inflow and, subsequently, the strength of the storm (Table 2) with the decrease in eddy diffusivity very similar to A100, A050, and A025 (Figs. 6 and 8). Initially smaller storms (S100, S050, and S025; Figs. 9d,e,f) show the same trend, indicating that the findings discussed in the earlier part of this study are not altered by some of the external factors that may affect storm size.
- A comparison between Figs. 2c,d,e with Figs. 9i,j,k in terms of wind speed at the 10-m level shows that intensification of the tropical cyclone inner core is initially stunted in a dryer environment. The inner core size is also further reduced in this case. While the minimum radius of the maximum winds during the lifetime of the TC in A025 was about 27 km at 48 hours, it was observed to be about 20 km at 72 hours in RHA025 (Table 2). Further, a comparison between simulations RHA100, RHA050, and RHA025 (Figs. 9i,j,k) indicates that there is a systematic increase in the strength of the inflow and, subsequently, in the strength of the storm (also refer to Table 2) with the decrease in eddy diffusivity very similar to A100, A050, and A025.

5. Summary and Conclusions

Recently, Gopalakrishnan et al. (2011a) studied the impacts of horizontal grid resolution on the intensification of an idealized tropical cyclone (TC) vortex. Based on a series of numerical experiments at the current operational model horizontal grid

resolution of about 9 km and at a finer experimental resolution of about 3 km, they found that the mature phase of the storm's evolution exhibited significantly different behavior with varying grid resolution. The axisymmetric budgets of radial and angular momentum revealed that the horizontal grid resolution had very little influence on the radial inflow and, subsequently, on the structure and storm "spin up" processes. However, radial gradients in the momentum budget provided the enhanced "spin up" mechanism at about 3-km resolution. Stronger convergence in the boundary layer led to improved transport of moisture fluxes and, subsequently, a stronger storm at higher resolution.

The present study illustrates that among the several internal factors that may influence the size and subsequent intensification of TCs, the PBL vertical diffusion appears to be the top candidate. The HWRF system uses the GFDL surface layer parameterization scheme and the MRF parameterization scheme where the eddy diffusivity for momentum is parameterized as $Km = k\,(U_*/\Phi_m)Z\,\{\alpha\,(1 - Z/h)^2\}$ in which k is the von Karman constant, U_* is the surface frictional velocity scale, Φ_m is the wind profile function evaluated at the top of the surface layer, Z is the height above the surface, and h is the boundary layer height. Eddy diffusivity of heat and moisture, Kh, is computed from Km using the relationship of the Prandtl number. Sensitivity experiments were conducted using the idealized HWRF framework, keeping the drag and enthalpy coefficients fixed and consistent with observations but varying the α parameter in the computation of the eddy diffusivities (Km and Kh). Flight-level data collected by a NOAA WP-3D research aircraft during the eyewall penetration of category 5 Hurricane Hugo (1989) at an altitude of about 450-500 m (Marks et al. 2008) and Hurricane Allen

(1980) (Marks 1985) were used as the basis to best match the modeled vertical eddy diffusivities with wind speed. The following are the salient results from this study:

- Reduction of Km (and Kh) to 25% of its original value produces reasonable diffusion coefficients consistent with observations for all wind speeds ranging from about 10 m s^{-1} to about 60 m s^{-1} in the MRF scheme.
- Reduction of Km has a significant influence on the structure, size, and evolution of the vortex. With Km set to 25% of its original value, the depth of the inflow layer is reduced from ~2 km to about 1 km, again, more consistent with the observations.
- As the inflow depth in the modeled storm is reduced to about 1 km, the radial inflow (cross-isobaric flow) is enhanced, leading, in turn, to an enhancement in the "spin up" of the primary circulation (specifically, tangential wind). The enhanced cross-isobaric flow also provides a mechanism for the transport of low-level θe air from the eyewall into the eye region. Although the surface evaporative fluxes are reduced by about 25% due to advection of moisture above the surface layer, the enhanced entropy (when compared to the baseline simulation) within the boundary layer is sufficient to enhance the efficiency of the hurricane heat engine.
- Stronger acceleration in the inflow leads to convergence farther inward before rising out of the boundary layer and ascending into the eyewall updraft and, consequently, a smaller storm in terms of the eyewall.
- Neither the initial vortex size nor the environmental relative humidity, which are known external factors that control the size of the storm, affect the above results.

- The structure of the PBL and the axisymmetric "spin up" of the idealized vortex discussed here appear to be more consistent with some of the observational (Zhang et al. 2011a,b) and theoretical (Montgomery and Smith 2011) modeling works that use a different parameterization scheme for vertical diffusion (e.g., Nolan et al. 2009a,b) when Km (and Kh) in the MRF scheme is reduced to 25% of its original value.

Bryan and Rotunno (2009) used an axisymmetric, non-hydrostatic numerical model to evaluate the maximum possible intensity of tropical cyclones. At a resolution of 1 km or less, the authors found significant sensitivity to the specification of turbulence intensity in their model. In particular, the authors concluded that the lateral diffusion in the model limits maximum intensity because it reduces the radial gradient of angular momentum, and turbulence also reduces radial gradients of θe (scalar). While other studies of both real and ideal cases show significant sensitivity to lateral diffusion (Gopalakrishnan et al. 2011b; Bao et al. 2011), we fixed the lateral diffusion to a minimum value recommended for the non-hydrostatic dynamic core (Janjic 1990) in the current work and instead varied the vertical diffusivity which also showed a sensitive dependence on the structure and intensity changes in the TCs. One of the sensitivity experiments of Bryan and Rotunno (2009), where the authors varied the vertical diffusivity, showed similar behavior (see Fig. 5 in their work). However, the run with smaller vertical diffusion produced an unrealistic value of radial inflow, as well as return flow above the boundary layer. Nevertheless, real hurricanes are three-dimensional, and perhaps the use of an axisymmetic model led to more unrealistic values in their study.

It should be mentioned that the current study is limited to numerical weather prediction models (NWP) for tropical cyclones, in which, turbulence is parameterized in terms of admittedly simplified parameters, rather than requiring such effects to be consequences of dynamics of the system (e.g. direct numerical simulations). While the vertical diffusion process is parameterized in terms of physical effects, the application of lateral diffusion in atmospheric models in general has always been a subject of debate since it is not clear to what extent one can model horizontal diffusion. Although it is not feasible to run direct numerical simulations even to understand the turbulence structure of tropical cyclones at this time, we believe that the use of observations to improve parameterization scheme in NWP applications especially for tropical cyclones is a realizable goal. Recent studies from Zhang et al. (2012) also provides an estimate of horizontal eddy diffusivity and mixing length in low-level region of intense hurricane. We are in the process of evaluating both the vertical and horizontal diffusivity in the HWRF system for real cases, as well.

Finally, the structure and intensification of modeled tropical cyclones are known to be sensitive to different parameterization schemes. A complementary study by Bao et al. (2011) discusses the sensitivity of the structure and intensification in an idealized developing tropical cyclone to various physics parameterization schemes in the HWRF system including microphysical and radiation parameterization schemes. The results presented here and in Bao et al. (2011) highlight the need for the research community to use structural metrics and better structural observations in its model evaluations to improve numerical models.

Acknowledgments:

The authors acknowledge funding from NOAA's Hurricane Forecast Improvement Project that supported this work. We acknowledge the contributions from Dr. Kao-San Yeh on the HWRF developmental efforts. Thanks are also due Drs. Robert Rogers and Young Kwon for providing a thorough internal review and insightful comments that led to significant improvements of the original manuscript. Thanks are due to Ms. Gail Derr for offering editorial support and to Mr. Arthur Eiserloh, a summer intern at NOAA who helped the primary author with the coding of the simple gradient wind equation that provided additional insights to this work.

References:

Anthes, R. A., and S. W. Chang, 1978: Response of the hurricane boundary layer to changes of sea-surface temperature in a numerical model. *J. Atmos. Sci.*, **35**, 1240-1255.

Bao, J.-W., S. G. Gopalakrishnan, S. A. Michelson, F. D. Marks, and M. T. Montgomery, 2011: Sensitivity of tropical cyclone structure and wind-pressure relationships to physics representations in the HWRFX model (communicated to *Mon. Wea. Rev.*).

Bell, M. M., and M. T. Montgomery, 2008: Observed structure, evolution, and potential intensity of category 5 Hurricane Isabel (2003) from 12-14 September. *Mon Wea. Rev.*, **136**, 2023-2046.

Bender, M. A., I. Ginis, R. E. Tuleya, B. Thomas, and T. Marchok, 2007: The operational GFDL coupled hurricane-ocean prediction system and a summary of its performance. *Mon. Wea. Rev.*, **135**, 3965-3989.

Black, P. G., and Coauthors, 2007: Air–sea exchange in hurricanes: Synthesis of observations from the Coupled Boundary Layer Air–Sea Transfer Experiment. *Bull. Amer. Meteor. Soc.*, **88**, 357–374.

.

Braun, S. A., and W.-K. Tao, 2000: Sensitivity of high-resolution simulations of Hurricane Bob (1991) to planetary boundary layer parameterizations. *Mon. Wea. Rev.*, **128**, 3941–3961.

Bryan, G. H., and R. Rotunno, 2009: The maximum intensity of tropical cyclones in axisymmetric numerical model simulations. *Mon. Wea. Rev.*, **137**, 1770-1789.

Cram, T. A., J. Persing, M. T. Montgomery, and S. A. Braun, 2007: A Lagrangian trajectory view on transport and mixing processes between the eye, eyewall, and environment using a high-resolution simulation of Hurricane Bonnie (1998). *J. Atmos. Sci.*, **64**, 1835–1856.

Donelan, M. A., B. K. Haus, N. Reul, W. J. Plant, M. Stiassnie, H. C. Graber, O. B. Brown, and E. S. Saltzman, 2004: On the limiting aerodynamic roughness of the ocean in very strong winds. *Geophys. Res. Lett.,* **31**, L18306, doi:10.1029/2004GL019460.

Emanuel, K. A., 1986: An air-sea interaction theory for tropical cyclones. Part I: Steady-state maintenance. *J. Atmos. Sci.,* **43**, 585–604.

Emanuel, K. A., 1995: Sensitivity of tropical cyclones to surface exchange coefficients and a revised steady-state model incorporating eye dynamics. *J. Atmos. Sci.,* **52**, 3969-3976.

Fels, S. B., and M. D. Schwarzkopf, 1975: The simplified exchange approximation: A new method for radiative transfer calculations. *J. Atmos. Sci.*, **32**, 1475–1488.

Ferrier, B. S., Y. Lin, T. Black, E. Rogers, and G. DiMego, 2002: Implementation of a new grid-scale cloud and precipitation scheme in the NCEP Eta model. *Preprints, 15th Conference on Numerical Weather Prediction, San Antonio, TX, Amer. Meteor. Soc.*, 280-283.

Gopalakrishnan, S., Q. Liu, T. Marchok, D. Sheinin, N. Surgi, R. Tuleya, R. Yablonsky, and X. Zhang, 2010: Hurricane Weather and Research and Forecasting (HWRF) model scientific documentation. L. Bernardet, Ed., 75 pp.

Gopalakrishnan, S. G., F. D. Marks, X. Zhang, J.-W. Bao, K.-S. Yeh, and R. Atlas, 2011a: The experimental HWRF system: A study on the influence of horizontal resolution on the structure and intensity changes in tropical cyclones using an idealized framework. *Mon. Wea. Rev.*, **139**, 1762-1784.

Gopalakrishnan, S. G., S. Goldenberg, T. Quirino, F. D. Marks, X. Zhang, K.-S. Yeh, R. Atlas, and V. Tallapragada, 2011b: Towards improving high-resolution numerical hurricane forecasting: Influence of model horizontal grid resolution, initialization, and physics. *Wea. Forecasting* (in press).

Gray, W. M., E. Ruprecht, and R. Phelps, 1975: Relative humidity in tropical weather systems. *Mon. Wea. Rev.*, **103**, 685-690.

Haus, B. K., D. Jeong, M. A. Donelan, J. A. Zhang, and I. Savelyev, 2010: Relative rates of sea-air heat transfer and frictional drag in very high winds. *Geophys. Res. Lett.*, **37**, L07802, doi:10.1029/2009GL042206.

Hong, S.-Y., and H.-L. Pan, 1996: Nonlocal boundary layer vertical diffusion in a medium-range forecast model. *Mon. Wea. Rev.*, **124**, 2322-2339.

Hong, S.-Y., and H.-L. Pan, 1998: Convective trigger function for a mass-flux cumulus parameterization scheme. *Mon. Wea. Rev.*, **129**, 1164-1178.

Janjic, Z. I., 1990: The step–mountain coordinates: Physical package. *Mon. Wea. Rev.*, **118**, 1429–1443.

Kepert, J. D., 2001: The dynamics of boundary layer jets within the tropical cyclone core. Part I: Linear theory. *J. Atmos. Sci.*, **58**, 2469–2484.

Kurihara, Y., and R. E. Tuleya, 1974: Structure of a tropical cyclone developed in a three-dimensional numerical simulation. *J. Atmos. Sci.*, **31**, 893–919.

Lacis, A. A., and J. E. Hansen, 1974: A parameterization for the absorption of solar radiation in the earth's atmosphere. *J. Atmos. Sci.*, **31**, 118–133.

Large, W. G., and S. Pond, 1981: Open ocean momentum flux measurements in moderate to strong winds. *J. Phys. Oceanogr.*, **11**, 324–336.

Malkus, J. S., and H. Riehl, 1960: On the dynamics and energy transformations in steady-state hurricanes. *Tellus*, **12**, 1-20.

Marks, F. D., 1985: Evolution of the structure of precipitation in Hurricane Allen (1980). *Mon. Wea. Rev.*, **113**, 909-930.

Marks, F. D., P. G. Black, M. T. Montgomery, and R. W. Burpee, 2008: Structure of the eye and eyewall of Hurricane Hugo (1989). *Mon. Wea. Rev.*, **136**, 1237–1259.

Montgomery, M. T., R. K. Smith, and S. Nguyen, 2010: Sensitivity of tropical cyclone models to the surface drag coefficient. *Quart. J. Roy. Meteor. Soc,* **136**, 1945-1953.

Montgomery, M. T., and R. K. Smith, 2011: Paradigms for tropical-cyclone intensification. *Quart. J. Roy. Meteor. Soc*, **137**, 1-31.

Moon, I.-J., T. Hara, I. Ginis, S. E. Belcher, and H. Tolman, 2004a: Effect of surface waves on air–sea momentum exchange. Part I: Effect of mature and growing seas. *J. Atmos. Sci.,* **61**, 2321–2333.

Moon, I.-J., I. Ginis, and T. Hara, 2004b: Effect of surface waves on air–sea momentum exchange. Part II: Behavior of drag coefficient under tropical cyclones. *J. Atmos. Sci.,* **61**, 2334–2348.

Nolan, D. S., J. A. Zhang, and D. P. Stern, 2009a: Evaluation of planetary boundary layer parameterizations in tropical cyclones by comparison of in-situ data and high-resolution simulations of Hurricane Isabel (2003). Part I: Initialization, maximum winds, and outer core boundary layer structure. *Mon. Wea. Rev.*, **137**, 3651–3674.

Nolan, D. S., J. A. Zhang, and D. P. Stern, 2009b: Evaluation of planetary boundary layer parameterizations in tropical cyclones by comparison of in-situ data and high-resolution simulations of Hurricane Isabel (2003). Part II: Inner core boundary layer and eyewall structure. *Mon. Wea. Rev.*, **137**, 3675–3698.

Ooyama, K. V., 1969: Numerical simulation of the life cycle of tropical cyclones. *J. Atmos. Sci.,* **26**, 3-40.

——, 1982: Conceptual evolution of the theory and modeling of the tropical cyclone. *J. Meteor. Soc. Japan,* **60**, 369–379.

Pan, H.-L., and J. Wu, 1995: Implementing a mass flux convection parameterization package for the NMC medium-range forecast model. NMC Office Note, No. 409, 40 pp. (available from NCEP, 5200 Auth Road, Washington, DC 20233).

Pattanayak, S., U. C. Mohanty, and S. G. Gopalakrishnan, 2011: Simulation of very severe Cyclone Mala over Bay of Bengal with HWRF modeling system. *J. Natural Hazards (Published online: June 9, 2011).*

Powell, M. D., P. J. Vickery, and T. Reinhold, 2003: Reduced drag coefficient for high wind speeds in tropical cyclones. *Nature*, **422**, 279-283.

Rosenthal, S. L., 1962: A theoretical analysis of the field motion in the hurricane boundary layer. National Hurricane Research Project, Report No. 56, US Dept of Commerce (available from NOAA/AOML, Hurricane Research Division, Miami, FL 33149-1026).

Schwarzkopf, M. D., and S. Fels, 1991: The simplified exchange method revisited: An accurate, rapid method for computation of infrared cooling rates and fluxes. *J. Geophys. Res.*, **96**, 9075-9096.

Smith, R. K., 1968: The surface boundary layer of a hurricane. *Tellus*, **20**, 473–483.

Smith, R. K., 2003: A simple model of the hurricane boundary layer. *Quart. J. Roy. Meteor. Soc.*, **129**, 1007–1027.

Smith, R. K., and S. Vogl, 2008: A simple model of the hurricane boundary layer revisited. *Quart. J. Roy. Meteor. Soc.*, **134**, 337–351.

Smith, R. K., M.T.Montgomery, and N. V. Sang, 2009: Tropical cyclone spin-up revisited. Quart. J. Roy. Meteor. Soc., 135, 1321–1335.

Smith, R. K., and G. L. Thomsen, 2010. Dependence of tropical-cyclone intensification on the boundary-layer representation in a numerical model. *Quart. J. Roy. Meteror. Soc.*, **136**, 1671-1685.

Stull, R. B., 2000: *Meteorology for Scientists and Engineers*. Second Edition, Brooks/Cole, Thomson Learning, Pacific Grove, 502 pp.

Tuleya, R. E., and Y. Kurihara, 1978: A numerical simulation of the landfall of tropical cyclones. *J. Atmos. Sci.*, **35**, 242-257.

Wang Y., 1995: On an inverse balance equation in sigma-coordinates for model initialization. *Mon. Wea. Rev.*, **123**, 482-488.

Willoughby, H. E., 1979: Forced secondary circulations in hurricanes. *J. Geophys. Res.*, **84**, 3173-3183.

Xu, J., and Y. Wang, 2010: Sensitivity of the simulated tropical cyclone inner-core size to the initial vortex size. *Mon. Wea. Rev*., **138**, 4135-4157.

Yeh, K.-S., X. Zhang, S. Gopalakrishnan, S. Aberson, R. Rogers, F. D. Marks, and R. Atlas, 2011: Performance of the experimental HWRF in the 2008 hurricane season. *J. Natural Hazards (Published online: March 24, 2011).*

Zhang, D.-L., Y. Liu, and M. K. Yau, 2001: A multiscale numerical study of Hurricane Andrew (1992). Part IV: Unbalanced flows. *Mon. Wea. Rev.*, **129**, 92-107.

Zhang, J., 2007: An airborne investigation of the atmospheric boundary layer structure in the hurricane force wind regime. *Doctoral Dissertation*, University of Miami, 149 pp.

Zhang, J. A., P. G. Black, J. R. French, and W. M. Drennan, 2008: First direct measurements of enthalpy flux in the hurricane boundary layer: The CBLAST results. *Geophys. Res. Lett.*, **35**, L14813, doi:10.1029/2008GL034374.

Zhang, J. A., F. D. Marks, M. T. Montgomery, and S. Lorsolo, 2011a: An estimation of turbulent characteristics in the low-level region of intense Hurricanes Allen (1980) and Hugo (1989). *Mon. Wea. Rev*., **139**, 1447-1462.

Zhang, J. A., R. F. Rogers, D. S. Nolan, and F. D. Marks, 2011b: On the characteristic height scales of the hurricane boundary layer. *Mon. Wea. Rev.*, **139**, 2523-2535.

Zhang, J. A. and M. Montgomery, 2011; Observational estimates of the horizontal eddy diffusivity and mixing length in the low-level region of intense hurricanes (In press, Journal of the Atmospheric Sciences)

Zhang, X., T. S. Quirino, S. Gopalakrishnan, K.-S. Yeh, F. D. Marks, and S. B. Goldenberg, 2011: HWRFX: Improving hurricane forecasts with high resolution modeling. *Comput. Sci. Eng.*, **13**, 13-21.

Figure Legends

Fig. 1. The variation of (a) drag coefficient (C_d) and (b) heat and moisture exchange coefficient (C_k) with 10-m wind speeds; high resolution HWRF model with 2010 upgrades (thick gray dots) from the control experiment (for α=1 in Table 1) compared with data from Large and Pond (1981), Powell et al. (2003), Donelan et al. (2004), Black et al. (2007), Zhang et al. (2008), and Haus et al. (2010).

Fig 2. Time history of the intensification process in an idealized storm for the three simulations provided in Table 1: (a) minimum mean sea level pressure in hPa, (b) radius of maximum wind at 10 m; Hovemoller diagram of the axisymmetric mean wind at a height of 10 m for (c) baseline simulation (α=1), (d) Km reduced to half (α=0.50), and (e) Km reduced to a quarter (α=0.25).

Fig. 3. The variation of the eddy diffusivity coefficient, Km, with 10-m wind speeds; high resolution HWRF model outputs from the (a) control experiment (α=1), (b) Km reduced to half (α=0.50), and (c) Km reduced to a quarter (α=0.25) compared with data from Zhang et al. (2011a).

Fig. 4. Tangentially averaged, 6-hourly time averaged, radius-height cross-section of the secondary circulation at 72 hours for (a) control (α=1), (b) Km reduced to half (α=0.50), and (c) Km reduced to a quarter (α=0.25). The black solid contour indicates the inflow, and the dotted contours show the outflow of the radial wind component (in m s^{-1}). Inflow is also shaded in colors. Only the lower 10 km has been expanded for convenience. The vertical velocity (in m s^{-1}) is shown by contour lines with updrafts indicted by green and weak subsidence indicated by yellow. Because the distribution of vertical velocity is skewed, please note that the scales are unequally spaced. For convenience, the vector field obtained that compounded the tangentially averaged vertical and the radial velocity components is also provided here. Presented in purple color are the estimates of the inflow layer depth from Zhang et al. (2011b).

Fig. 5. Influence of the inflow layer depth on the PBL winds in a hurricane. Variations of tangential and radial inflow obtained for various inflow layer depths and for different Cd values obtained from a simple model that provides iterative solutions to the boundary-layer gradient (BLG) wind equations. This simple model was developed and used as the basis to explain some of the more complex solutions obtained from the HWRF system discussed in this work.

Fig. 6. Hovemoller diagram of the tangentially averaged, 6-hourly time averaged radial component of velocity (in ms^{-1}). Superposed on the contour lines is the generalized Coriolis term (i.e., Term A in equation 2 in text) *with the addition of a frictional effect* shaded in color for the HWRF runs with (i) α=1, (ii) α=0.5, and (iii) α=0.25 runs at the 30-m level. The blue end of the spectrum represents tangential acceleration (contributing

towards the "spin up"), and the red end of the spectrum represents deceleration within the inner eyewall region. Units of the forcing term are in m s^{-1} h^{-1}.

Fig. 7. Provides the Hovemoller diagram of the tangentially averaged, 6-hourly time averaged radial θ_e at the 30-m level for the HWRF runs with (i) α=1 (A100), (ii) α=0.5 (A050), and (iii) α=0.25 (A025). The region of vertical motion exceeding the 0.2 m s^{-1} contour line at the top of the boundary layer is shown to indicate the approximate region of eyewall convection.

Fig. 8. Hovemoller diagram of the tangentially averaged, 6-hourly time averaged radial component of velocity (in m s^{-1}). Superposed on the contour lines in shaded color is the net radial radial forcing term *including radial friction* in the governing equation for the secondary circulation (equation 2) for the HWRF runs with (i) α=1, (ii) α=0.5, and (iii) α=0.25 runs at the 30-m level. The blue end of the spectrum represents radial acceleration (convergence), and the red end of the spectrum represents deceleration within the inner eyewall region. Units of the net radial radial forcing term are in m s^{-1} h^{-1}.

Fig. 9. Hovemoller diagram of the axisymmetric mean winds (m s^{-1}) at a height of 10 m. Contour lines representing the tangentially averaged, 6-hourly time averaged radial component of velocity (in m s^{-1}) at 30-m level are superposed. Top row (a), (b), and (c) are sensitivity experiments for an initially big vortex (experiments 4, 5, and 6 in Table 1). Middle row (c), (d), and (e) are sensitivity experiments for initially small vortex (experiments 7, 8, and 9 in Table 1) and bottom row (f), (g), and (h) are sensitivity experiments in which the relative humidity of the large scale environment was reduced to about 50% from the baseline Jordan sounding. The radius of the initial vortex size for the experiments illustrated in the bottom row (f, g, and h) was set to the base value, i.e., 90 Km (Table 1).

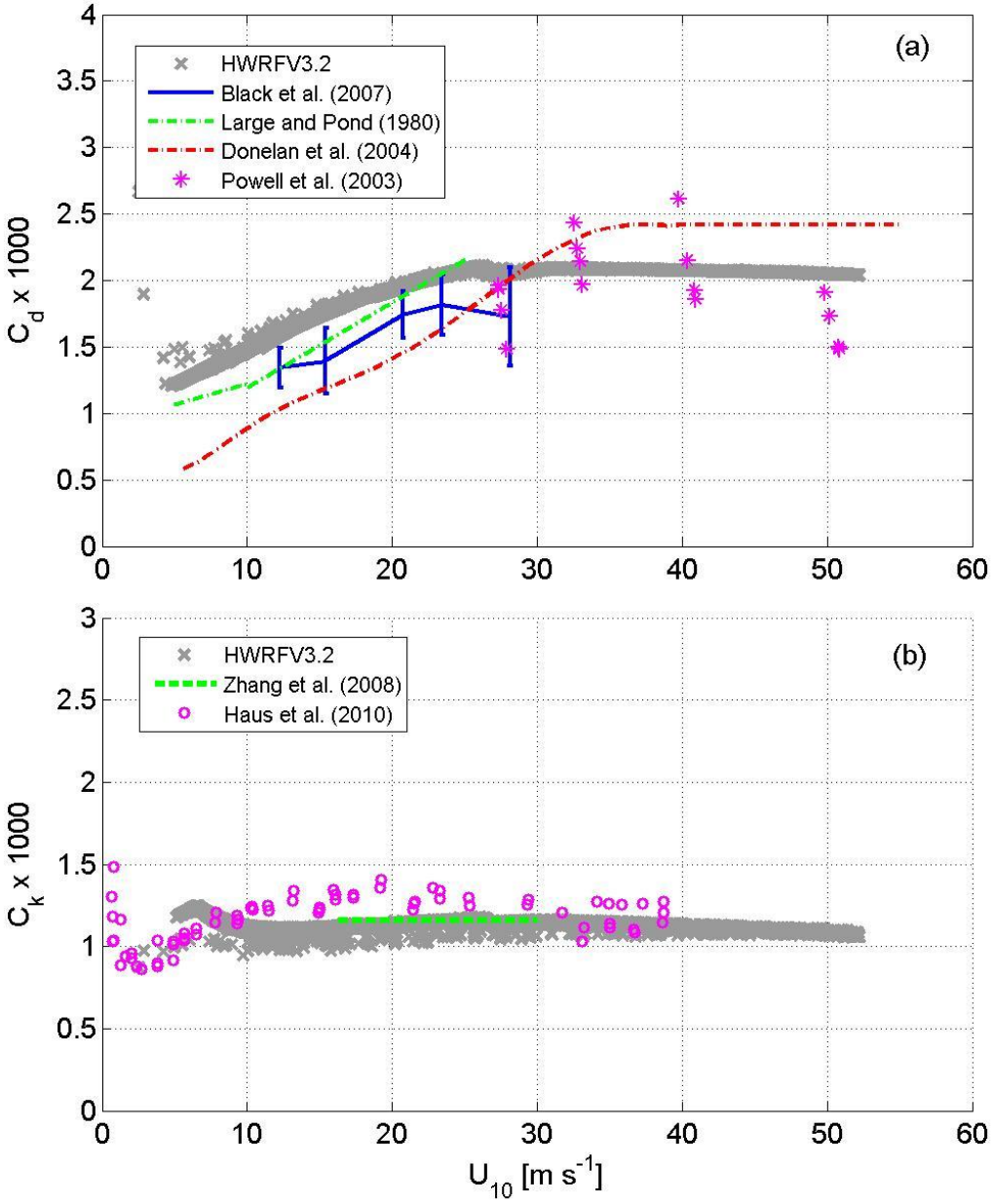

Fig. 1. The variation of (a) drag coefficient (C_d) and (b) heat and moisture exchange coefficient (C_k) with 10-m wind speeds; high resolution HWRF model with 2010 upgrades (thick gray dots) from the control experiment (for α=1 in Table 1) compared with data from Large and Pond (1981), Powell et al. (2003), Donelan et al. (2004), Black et al. (2007), Zhang et al. (2008), and Haus et al. (2010).

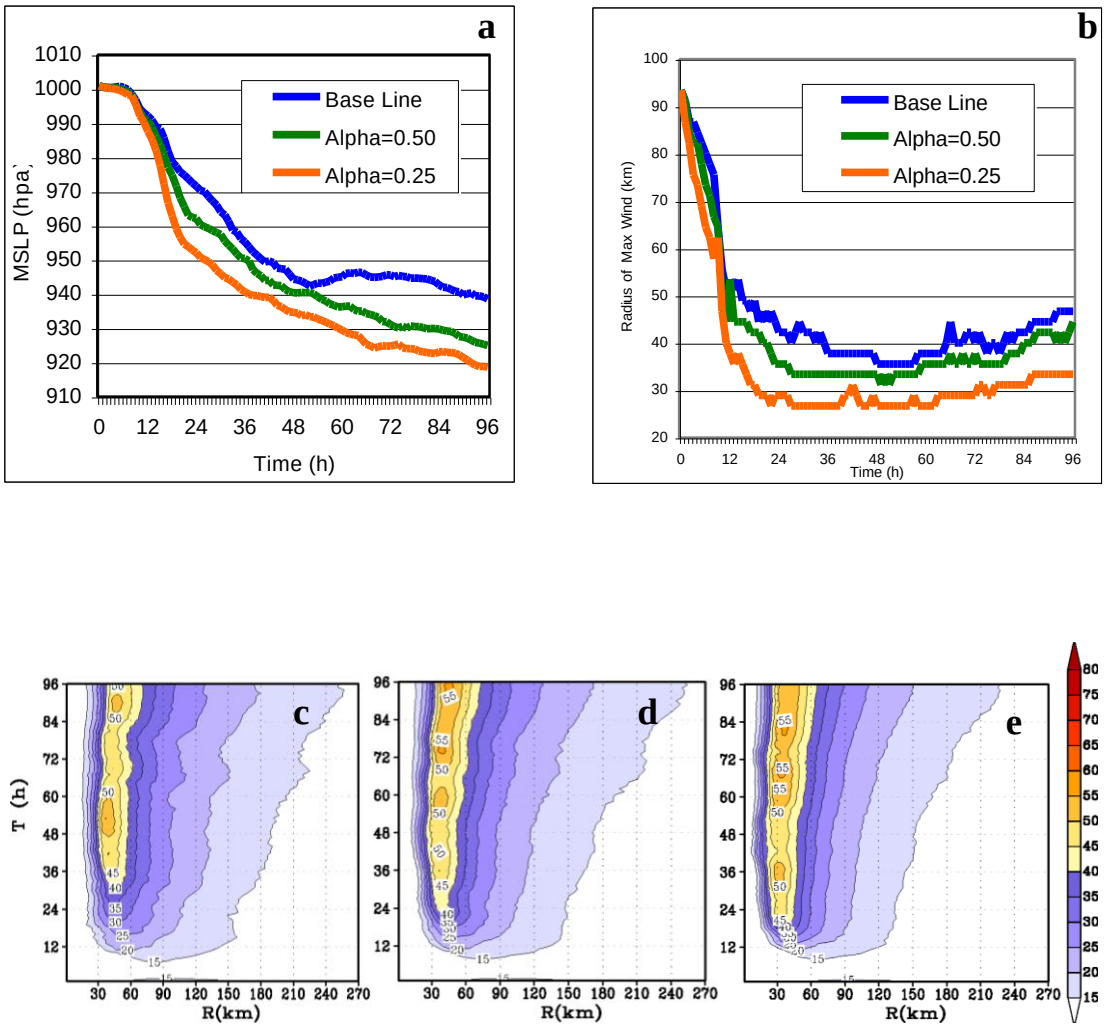

Fig 2. Time history of the intensification process in an idealized storm for the three simulations provided in Table 1: (a) minimum mean sea level pressure in hPa, (b) radius of maximum wind at 10 m; Hovemoller diagram of the axisymmetric mean wind at a height of 10 m for (c) baseline simulation (α=1), (d) Km reduced to half (α=0.50), and (e) Km reduced to a quarter (α=0.25).

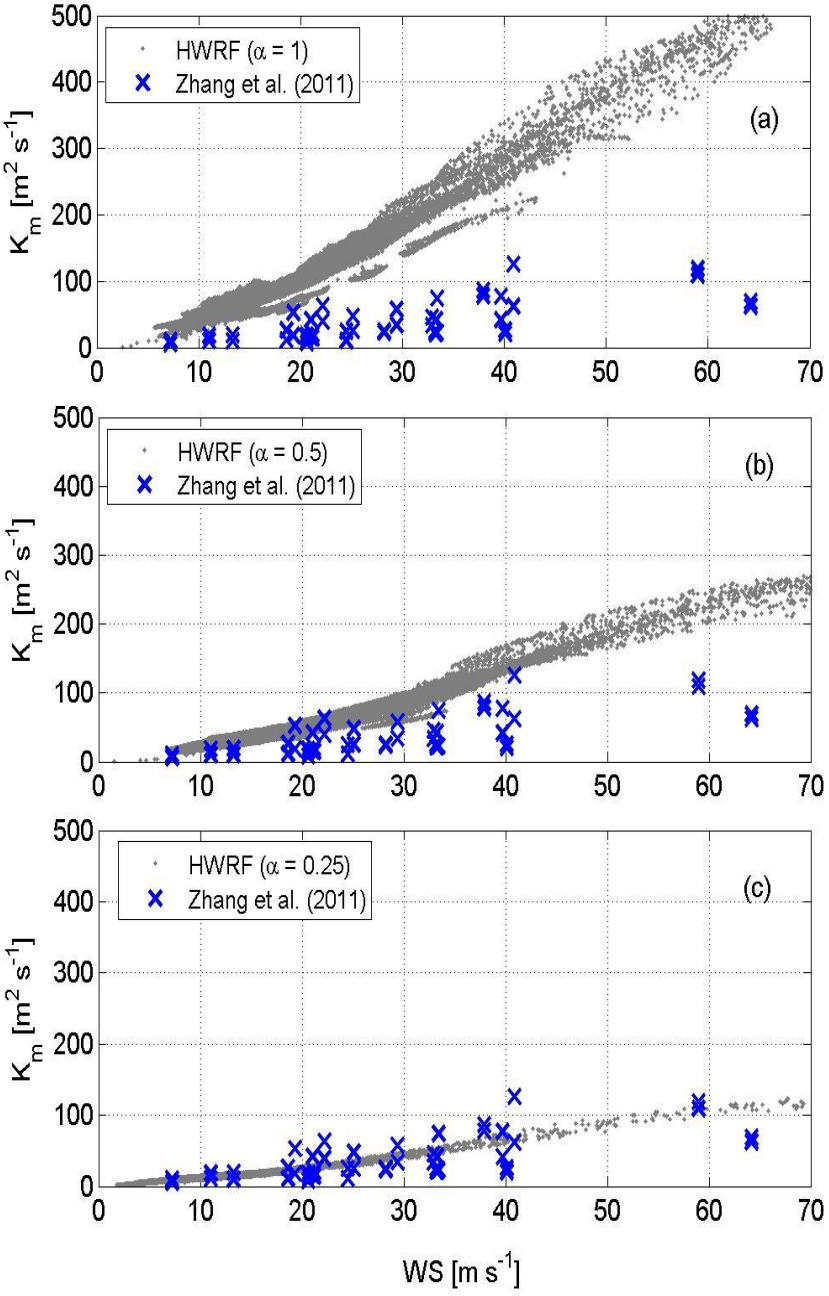

Fig. 3. The variation of the eddy diffusivity coefficient, Km, with 10-m wind speeds; high resolution HWRF model outputs from the (a) control experiment (α=1), (b) Km reduced to half (α=0.50), and (c) Km reduced to a quarter (α=0.25) compared with data from Zhang et al. (2011a).

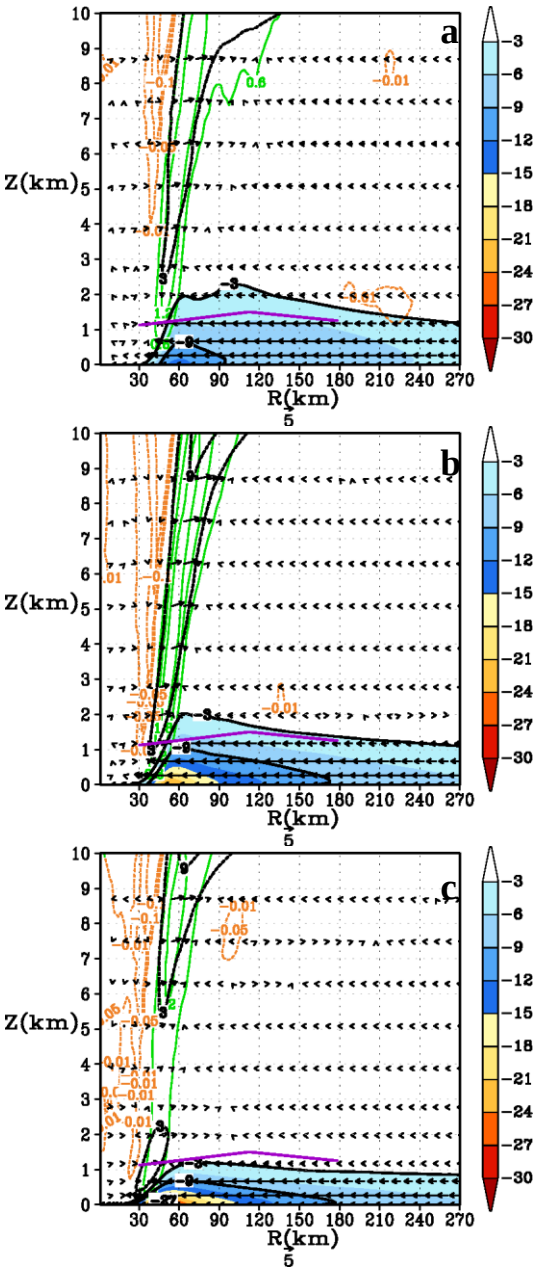

Fig. 4. Tangentially averaged, 6-hourly time averaged, radius-height cross-section of the secondary circulation at 93 hours for (a) control (α=1), (b) Km reduced to half (α=0.50), and (c) Km reduced to a quarter (α=0.25). The black solid contour indicates the inflow, and the dotted contours show the outflow of the radial wind component (in m s^{-1}). Inflow is also shaded in colors. Only the lower 10 km has been expanded for convenience. The vertical velocity (in m s^{-1}) is shown by contour lines with updrafts indicted by green and weak subsidence indicated by yellow. Because the distribution of vertical velocity is skewed, please note that the scales are unequally spaced. For convenience, the vector field obtained that compounded the tangentially averaged vertical and the radial velocity components is also provided here. Presented in purple color are the estimates of the inflow layer depth from Zhang et al. (2011b).

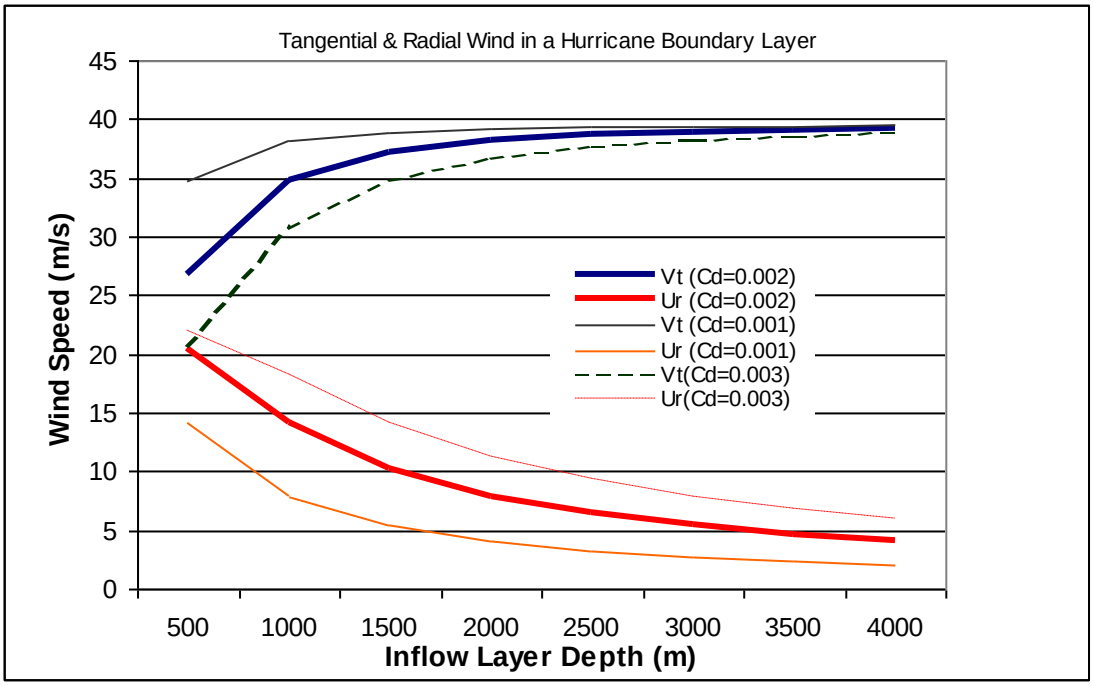

Fig. 5. Influence of the inflow layer depth on the PBL winds in a hurricane. Variations of tangential and radial inflow obtained for various inflow layer depths and for different Cd values obtained from a simple model that provides iterative solutions to the boundary-layer gradient (BLG) wind equations. This simple model was developed and used as the basis to explain some of the more complex solutions obtained from the HWRF system discussed in this work.

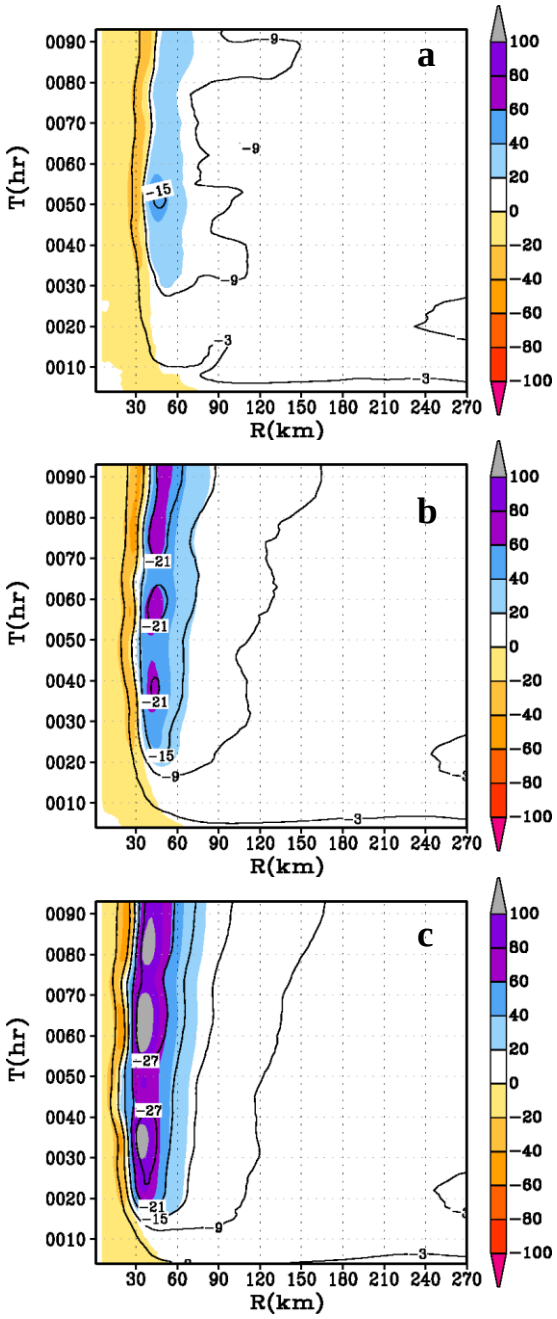

Fig. 6. Hovemoller diagram of the tangentially averaged, 6-hourly time averaged radial component of velocity (in ms^{-1}). Superposed on the contour lines is the generalized Coriolis term (i.e., Term A in equation 2 in text) *with the addition of a frictional effect* shaded in color for the HWRF runs with (i) α=1, (ii) α=0.5, and (iii) α=0.25 runs at the 30-m level. The blue end of the spectrum represents tangential acceleration (contributing towards the "spin up"), and the red end of the spectrum represents deceleration within the inner eyewall region. Units of the forcing term are in m s^{-1} h^{-1}.

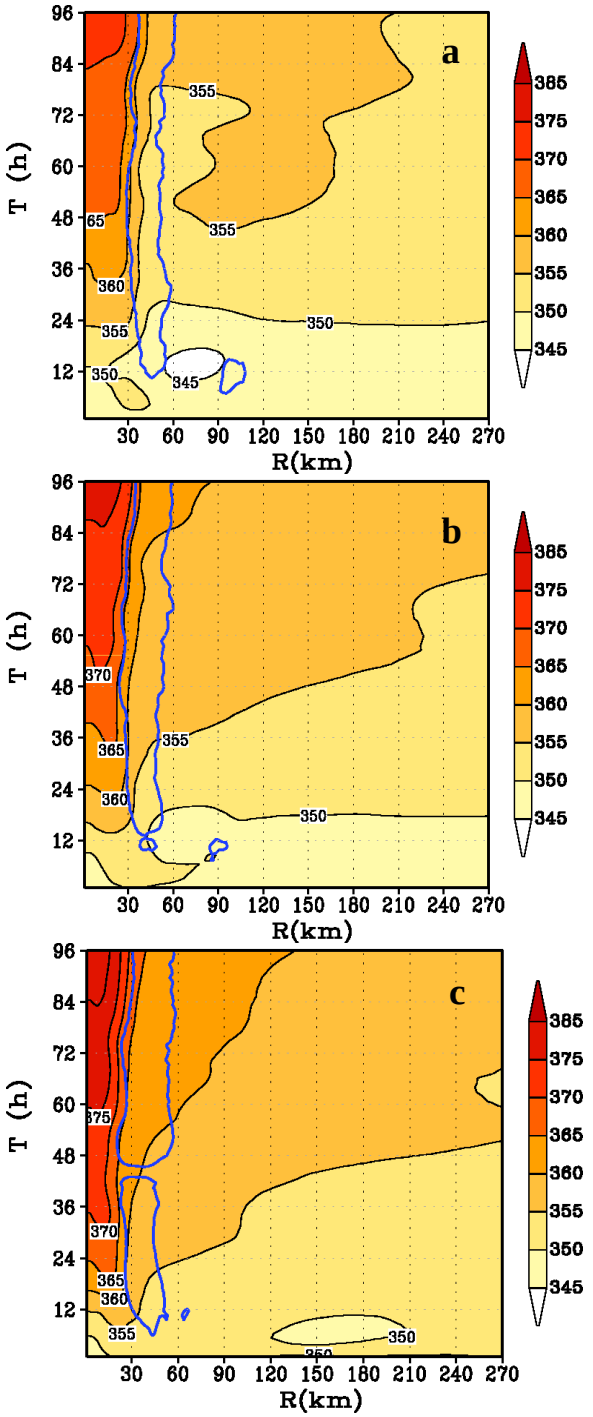

Fig. 7. Provides the Hovemoller diagram of the tangentially averaged, 6-hourly time averaged radial θ_e at the 30-m level for the HWRF runs with (i) α=1 (A100), (ii) α=0.5 (A050), and (iii) α=0.25 (A025). The region of vertical motion exceeding the 0.2 m s^{-1} contour line at the top of the boundary layer is shown to indicate the approximate region of eyewall convection.

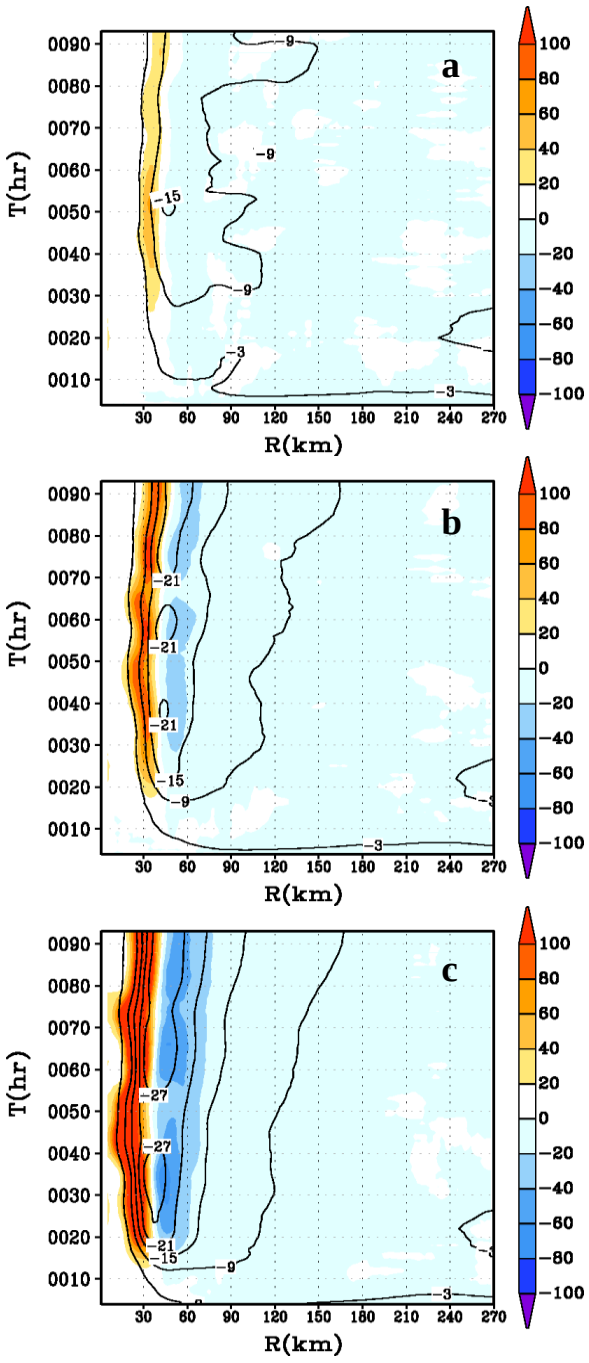

Fig. 8. Hovemoller diagram of the tangentially averaged, 6-hourly time averaged radial component of velocity (in m s^{-1}). Superposed on the contour lines in shaded color is the net radial radial forcing term *including radial friction* in the governing equation for the secondary circulation (equation 2) for the HWRF runs with (i) α=1, (ii) α=0.5, and (iii) α=0.25 runs at the 30-m level. The blue end of the spectrum represents radial acceleration (convergence), and the red end of the spectrum represents deceleration within the inner eyewall region. Units of the net radial radial forcing term are in m s^{-1} h^{-1}.

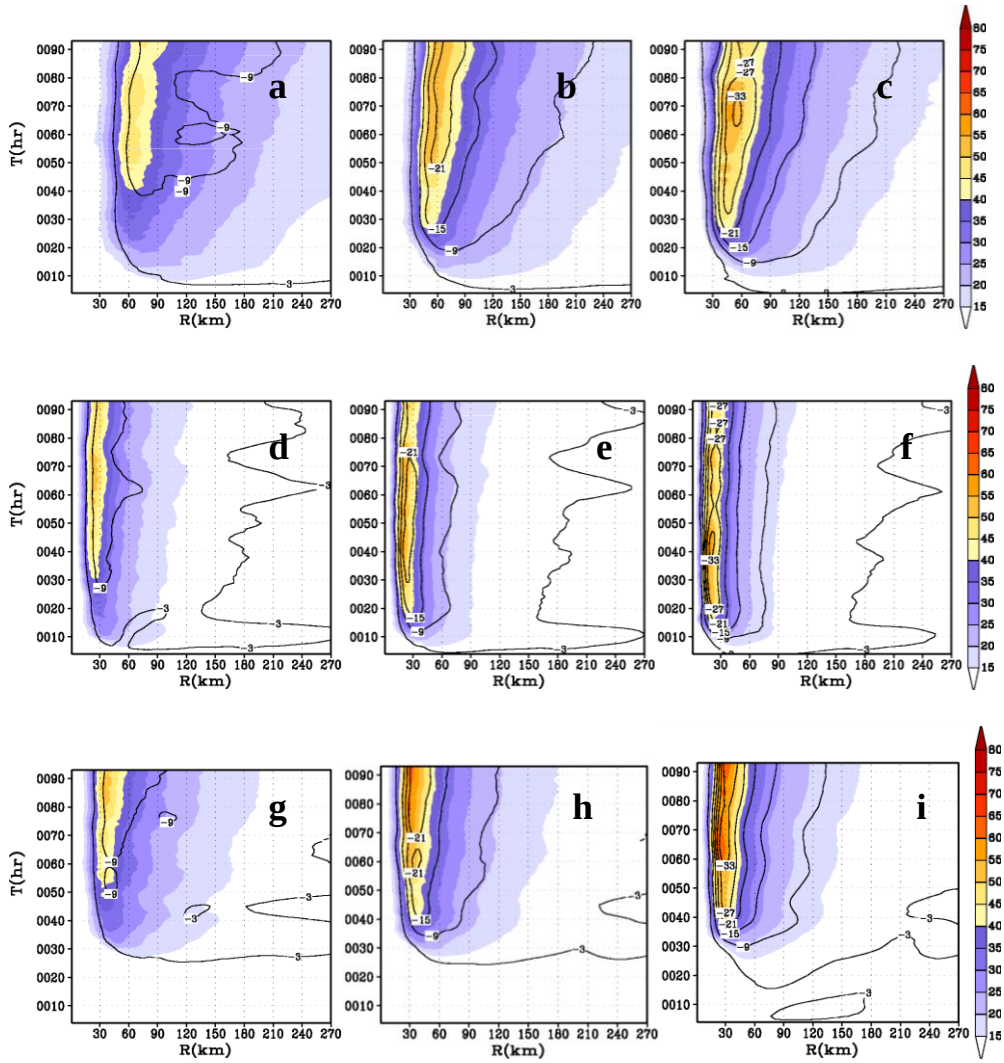

Fig. 9. Hovemoller diagram of the axisymmetric mean winds (m s^{-1}) at a height of 10 m. Contour lines representing the tangentially averaged, 6-hourly time averaged radial component of velocity (in m s^{-1}) at 30-m level are superposed. Top row (a), (b), and (c) are sensitivity experiments for an initially big vortex (experiments 4, 5, and 6 in Table 1). Middle row (d), (e), and (f) are sensitivity experiments for initially small vortex (experiments 7, 8, and 9 in Table 1) and bottom row (g), (h), and (i) are sensitivity experiments in which the relative humidity of the large scale environment was reduced to about 50% from the baseline Jordan sounding. The radius of the initial vortex size for the experiments illustrated in the bottom row (g, h and i) was set to the base value, i.e., 90 km (Table 1).

1

2 Table 1: List of experiments performed

Expt. No	Initial Radius of Maximum Wind (km)	Relative Humidity	Description	Specification	Remarks
1	90	Jordan	α=1.00	A100	Baseline Km & Kh in MRF
2	90	Jordan	α=0.50	A050	Km,Kh reduced to half
3	90	Jordan	α=0.25	A025	Km,Kh reduced to a quarter
4	120	Jordan	α=1.00	B100	Big storm; baseline Km, Kh
5	120	Jordan	α=0.50	B050	Big storm; half Km, Kh
6	120	Jordan	α=0.25	B025	Big storm; quarter Km, Kh
7	60	Jordan	α=1.00	S100	Small storm; baseline Km, Kh
8	60	Jordan	α=0.50	S050	Small storm; half Km, Kh
9	60	Jordan	α=0.25	S025	Small storm; quarter Km, Kh
10	90	50% Jordan	α=1.00	RHA100	Dry storm; baseline Km, Kh
11	90	50% Jordan	α=0.50	RHA050	Dry storm; half Km, Kh
12	90	50% Jordan	α=0.25	RHA025	Dry storm; quarter Km, Kh

3

4

5 Table 2: Simulation statistics gathered during the life time of the storm.

Expt. No	Specification	Minimum MSLP (hPa)	Maximum 10-m Wind Speed (ms^{-1})	Maximum Tangential Wind (ms^{-1})	Radius of maximum wind (km)
1	A100	939	60	70	36
2	A050	925	62	76	31
3	A025	919	63	79	27
4	B100	941	58	64	56
5	B050	928	61	76	45
6	B025	918	62	83	36
7	S100	942	61	64	20
8	S050	935	62	73	16
9	S025	932	62	76	13
10	RHA100	942	62	66	31
11	RHA050	924	68	79	25
12	RHA025	916	69	87	20

6
7
8

Figure1
Click here to download Non-Rendered Figure: Figure1.doc

Figure2
Click here to download Non-Rendered Figure: Figure2.doc

Figure3
Click here to download Non-Rendered Figure: Figure3.doc

Figure4
Click here to download Non-Rendered Figure: Figure4.doc

Figure5
Click here to download Non-Rendered Figure: Figure5.doc

Figure6
Click here to download Non-Rendered Figure: Figure6.doc

Figure7
Click here to download Non-Rendered Figure: Figure7.doc

Figure8
Click here to download Non-Rendered Figure: Figure8.doc

Figure9
Click here to download Non-Rendered Figure: Figure9.doc